# Measuring Ions with Scanning Ion Conductance Microscopy

*by Lushan Zhou, Yi Zhou, and Lane A. Baker*

The opportunity to position a small electrode at an interface with high accuracy and precision has led to important advances in surface electrochemical measurements and has made scanned probe microscopies (SPMs) an indispensable tool for the electrochemist. Scanning electrochemical microscopy (SECM)[1-8] has been a key SPM for electrochemists, and has found wide implementation in subjects that range from battery science[9] to bacterial communication.[10] A similar technique, scanning ion conductance microscopy (SICM),[11] was introduced by Hansma and coworkers around the same time as SECM was first reported, but wasn't really appreciated by the electrochemical community to the same degree. The lack of adoption of SICM stemmed from several issues, including the lack of chemical specificity exhibited and the less quantitative mathematical descriptions of the processes involved. Seminal efforts of Korchev and Klenerman to develop SICM further, notably in hardware and imaging protocols for biological systems, provided quantum leaps in methods available.[12] More recently, other groups have taken advantage of electrochemical measurements that might be afforded by SICM. Here, in context of the larger body of work, we describe some of our recent efforts in electroanalysis with SICM.

## Scanning Ion Conductance Microscopy in Ion Transport Studies

In their original report, Hansma and coworkers realized the possibilities of measuring ion transport with SICM, and stated: *"The most promising application for the SICM is not, however, just imaging the topography of surfaces at submicrometer resolution. The SICM can image not only the topography, but also the local ion currents coming out through pores in a surface."*[11] Measuring local ion transport at small scales can lead to insight for both fundamental studies and technological applications. For instance, in biological measurements, studies of ion transport through protein channels in cells have informed understanding of biological processes such as cell signaling and regulation of cell volume. Further applications of ion transport measurements include microfluidic separations, biosensors, and lithium-ion batteries. In SICM (shown as a cartoon in Fig. 1, left) a pipette with a small tip diameter (Fig. 1, middle) is scanned over the surface of a sample in electrolyte solution. A potential difference is applied between an electrode inside the pipette and an electrode in the outside bath solution, which results in an ion current that flows through the pipette. As the pipette is moved to the sample surface, resistance that develops in the gap between the pipette tip and sample affects the ion current through the pipette, which provides the feedback signal required for imaging/probe positioning. This mode of feedback for SICM is similar to the negative-feedback mode of SECM, where the gap between the shroud surrounding the electrode and the surface restricts diffusion of redox species to the electrode, resulting in a distance-dependent current.[2] In practice, more complicated feedback modes are typically used for SICM, but conceptually the same phenomena are utilized. Topographic images of the surface can be generated from scanning the pipette over a surface while maintaining constant probe-sample distance. Additionally, local conductance measurements can be performed with high spatial resolution.

SICM is an attractive tool for nanoscale ion transport studies, especially for studies of biological samples, for a number of reasons. First, typical spatial resolution of SICM can be < 10 nm vertically and < 50 nm laterally, as determined by the pipette geometry. Second, redox mediators are not required for imaging, as SICM measures the local conductivity, or total ion concentration. Third, SICM works exceptionally well in electrolyte solutions required to maintain

*(continued on next page)*

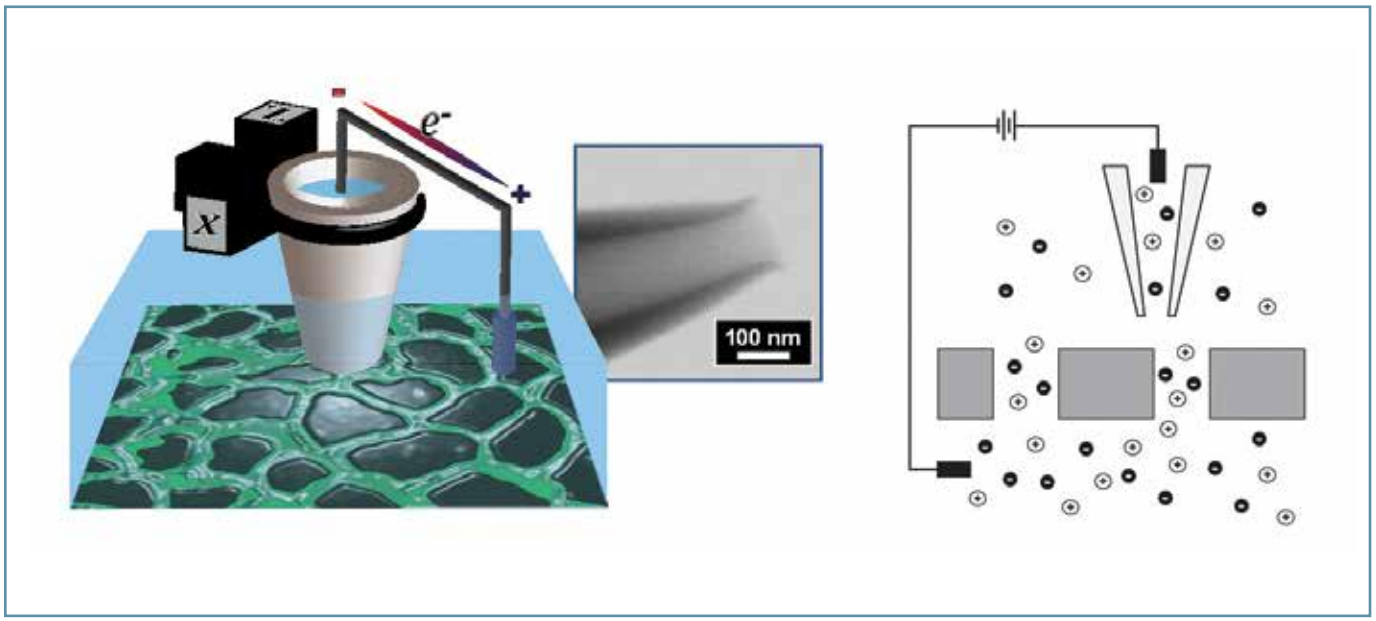


**Fig. 1.** *Cartoon schematic of scanning ion conductance microscopy (SICM) (left). Center inset shows a scanning transmission electron micrograph of a typical nanopipette tip utilized for SICM. Right schematic shows a general experimental setup for measuring ion currents at synthetic membranes with SICM. (Portions of figure adapted with permission from reference [13].)*

biological samples. Finally, probes with small tip diameters (nanopipettes) can be fabricated easily by pulling glass/quartz capillaries, and these probes can be further modified to monitor additional signals such as potential or faradaic electron transfer. With these advantages, SICM has proved a versatile tool to study ion transport in various systems that span from porous polymer membranes to living cells.[13-22]

## Control of Ion Transport through Synthetic Nanopores

For fundamental studies, artificial nanopores have advantages such as stability, controllable and well-defined size and shape, and ease of fabrication. To date, many nanofabrication techniques for nanopore synthesis have been reported, such as the track-etch process, ion beam sputtering, and electron beam lithography. Porous (poly) imide membranes with nanopore diameters that range from tens to hundreds of nanometers have been the platform of choice in our lab and are prepared by chemical etching of ion-tracked polymer foils.

SICM is able to generate a topographic image and current image of porous membranes simultaneously, from which the position and conductance of nanopores can be measured. To further study ion-transport properties of nanopores, a concentration gradient or a potential applied across the membrane can be used to drive diffusion and migration of ions.

## Diffusion-Driven Ion Transport

In the simplest case of diffusion-driven ion transport (Fig. 1, right), a membrane with cylindrical nanopores was mounted between the upper and lower chambers of a perfusion cell.[11] Electrolyte (KCl) concentration in the lower chamber was varied from 0.1 to 4.0 M, while the electrolyte concentration in the upper chamber was maintained at 0.1 M. This concentration difference between the two chambers resulted in an ion current through pores in the membrane. A linear relationship between ion current and transmembrane concentration difference was observed for different pore sizes (300 nm and 500 nm). Alteration of pore sizes resulted in measured differences in ion currents, fundamentally related to the mass-transfer resistance determined by the pore structure. Current profiles across the nanopores were measured and modeled with the Goldman-Hodgkin-Katz (GHK) equation,[23] which describes diffusive ion flux ($j$) of an ion with diffusion coefficient ($D$) driven by concentration gradient ($CL - CU$) through a membrane of thickness $L$, equation (1).

$$j_{\pm} = \frac{\mp D_{\pm}\Delta}{L}\left(\frac{C_s^L}{1-e^{\mp\Delta}} - \frac{C_s^U}{e^{\pm\Delta}-1}\right) \quad (1)$$

Deviations from the GHK model were observed for "normalized ion current – transmembrane concentration difference" relationships, presumably due to convection induced by vertical modulation of the SICM pipette (these experiments used an "AC" feedback mode).[24] In an effort to obtain more quantitative information, methods to perform conductance measurements at fixed positions were developed for subsequent ion conductance measurements.

## Migration-Driven Ion Transport

In the case of migration-driven transport, additional electrodes were added to the system to apply a transmembrane potential, to result in three- and four-electrode SICM configurations.[15,22] First, a "working electrode" (Ag/AgCl) was added.[15] Here experiments were setup in the same way as the case described above, except that the concentrations on each side of the membrane were held constant, and a transmembrane potential was applied at the working electrode to control the electric field at nanopores. Localized current-voltage responses were measured for a single nanopore by sweeping the transmembrane potential when the pipette was held over the center of the nanopore and observing the response at the SICM pipette electrode. Current response of the single nanopore was evaluated with a circuit model, which validated the response measured by the SICM pipette. In addition, nanopipettes were positioned inside nanopores to measure vertical distribution of the current-voltage response, and enhanced interactions between the charged walls of the pipette and the pore were observed from increases in the access resistance measured. Localized current-voltage responses recorded with this setup were further utilized to characterize pore geometry. The extent of current rectification for membranes with conical nanopores was also measured with the instrumentation described above, and further demonstrated how the measurement reflected the conductance properties of the membrane/nanopore under study.

To study heterogeneity of ion transport pathways further, a counter electrode was added to handle the higher currents passed by less resistive membranes.[22] With this four-electrode configuration of SICM, heterogeneous ion conductance of individual pores in a multi-pore membrane could be measured. In these experiments, marked differences in rectification was observed for pores prepared in the same membrane, which suggested that a distribution of pore geometries or surface chemistries exists.

In the studies described above, we demonstrated that local conductance pathways can be recorded with SICM, and that changes in ion transport via concentration gradients or transmembrane potential could be observed with SICM. However, limitations to the application of these techniques in naturally occurring nanopores such as ion pathways in the cell membrane still exist, most of which are signal-to-noise related. For example, high salt concentrations (>1.0 M) or high transmembrane potentials (>500 mV) were required to generate sufficient current signals. To address some of these limitations, potentiometric SICM was developed.

## Potentiometric Measurements with SICM

In all of this work, one of our goals has been to adapt SICM to more facile measurements of ion current at biological interfaces. To develop SICM in this venue, we adopted the concept of voltage scanning, first introduced by Frömter in 1972.[25] In voltage scanning, the local current density over different conductive pathways of a cell membrane is measured by control of the position of a micropipette over said pathways.[25-35] In these measurements, recording changes in the voltage or potential at the tip of the pipette leads to more sensitive measurements, especially when the limiting diameter of the pipette becomes very small (resistance of a typical SICM nanopipette ~ MΩ). In our work, we coupled this type of potentiometric measurement to the SICM configuration described above, to result in what we term potentiometric-SICM (P-SICM, Fig. 2, top left).[16] Advantages of P-SICM include: (1) high resolution images of the cell layer can be used to locate features of interest, and (2) precise pipette position is achieved with feedback control.

In P-SICM, a dual-barrel nanopipette is utilized as the probe. One barrel serves to measure ion current as a feedback signal for SICM and control tip position. The second barrel measures local potential in the vicinity of the pipette tip. To realize this tool and control potentials across the sample, additional electrodes were used in a manner similar to that described previously. Topographic ion current and potential images of the sample can be generated simultaneously with P-SICM. The signal-to-noise ratio attained for P-SICM was 4-5 times higher than the typical current measurement (Fig. 2, top right), which enables measurement of local conductance for biological samples.

P-SICM was utilized to study ion transport pathways in wild type Madin-Darby canine kidney strain II (MDCKII-WT) cells. High-resolution topographic images of the cell surface were generated first with the SICM (Fig. 2, bottom left). Two different ion transport pathways: paracellular pathways at cell junctions (CJ) and transcellular pathways at cell bodies (CB), were of interest in these studies. To assess conductance in these locations, the pipette was positioned over these locations (CBs or CJs) to record local conductance values. As addressed above, fixed position measurements, in which the probe is held at constant height above a feature of interest and the current or potential response

are recorded, were then performed with P-SICM. To calculate the local conductance, potential deflection was measured at two probe-sample distances ($D_{ps}$), one close to the sample surface ($D_{ps}$ = 0.2 µm) and one far away from the sample ($D_{ps}$ = 12.5 µm). Equation (2)[24,32] was then used to calculate the apparent local conductances,

$$G = \left(\frac{E}{\rho \cdot V^e}\right) = \left(\frac{\left(\Delta V_{0.2\mu m} - \Delta V_{12.5\mu m}\right)/\Delta z}{\rho \cdot V^e}\right) \quad (2)$$

where the electric field (E, a potential gradient) was determined by dividing the potential difference ($\Delta V_{0.2\mu m} - \Delta V_{12.5\mu m}$) recorded at two distinct pipette distances ($D_{ps}$) by the vertical displacement of the pipette ($\Delta z$). Here, ρ is the specific resistance of the bath electrolyte and $V^e$ is the potential range applied at WE (Fig. 2c) to induce potential deflections. Apparent conductance (G) over CBs (transcellular) and CJs (paracellular) showed average values of 2.53 ± 1.49 mS/cm² (n = 49) and 6.20 ± 2.54 mS/cm² (n = 62), respectively. Statistical analysis showed that the transcellular conductance ($G^t$) differed significantly from the paracellular conductance ($G^p$) ($p < 0.001$), in good agreement with values reported previously for MDCKII-WT cells. Further, a siRNA knockdown MDCKII cell line, in which the expression of a paracellular channel protein claudin-2 is depressed (MDCKII-C2 cell), was tested with P-SICM. The $G^p$ in MDCKII-C2 cells decreased to 2.63 ± 1.26 mS/cm² (n = 78), compared to 6.20 ± 2.54 mS/cm² (n = 62) in WT cells (Fig. 2, lower right). This result showed that P-SICM could be used to measure the local conductance changes in polarized epithelia and holds promise for measurement of ion transport in complex, functional, living systems.

## Toward Chemical Selectivity in SICM

A criticism of SICM is the lack of chemical specificity. We realized that when a nanopipette is brought close to a surface, the electrostatic charge on the nanopipette

*(continued on next page)*

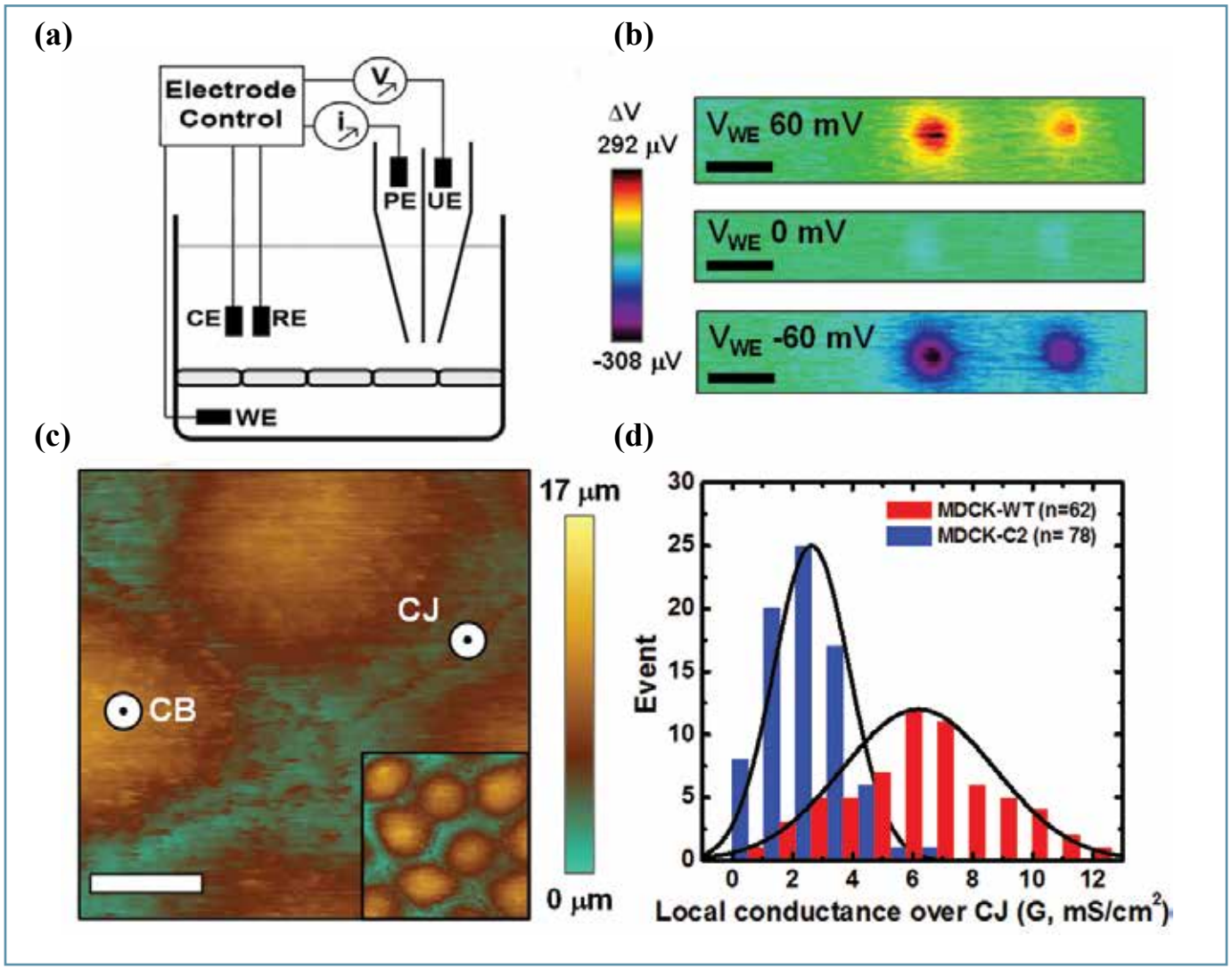


**Fig. 2.** *(a) Illustration of potentiometric scanning ion conductance microscopy (P-SICM). A dual-barrel pipette is utilized to measure topographic and potential gradients of a sample of interest. Here the pipette electrode (PE) is used to control pipette position and record topographic images. The potentiometric electrode (UE) records the local potential at the pipette tip. A potential is applied across the sample between the working electrode (WE) and counter electrode (CE). All electrode potentials are referenced to a common reference electrode (RE). Characterization of porous membranes with P-SICM. (b) Images of local potential variations for these two pores at a series of transmembrane potentials ($V_{TM}$), recorded with P-SICM in imaging mode (Scale bar = 1 µm). (c) Topographic image of the apical surface of a cell monolayer was imaged to locate the position of cell bodies and the cell junctions. Scale bar: 5 µm. The inset shows the zoom out image of the cell monolayer under study (40 x 40 µm). Two positions which illustrate pipette placement are indicated for CB (cell body) and CJ (cell junction). The black marker in the center of the larger white marker at these positions approximates the size of the pipette tip utilized. (d) Histogram of conductances recorded over CJs for MDCKII-WT (red) presents a broader distribution with a larger mean value, as compared to that of MDCKII-C2 (blue). These observations indicate that claudin-2 functions to regulate the epithelial permeability through paracellular pathways. (Portions of figure and caption adapted with permission from reference [16].)*

*(continued from previous page)*

and surface might preferentially influence the transport of cations or anions in a selective or predictable fashion. Toward this goal, we demonstrated transduction of the charge on a surface when nanopipettes are held at distances on the order of ten to hundreds of nanometers from the surface of interest. Rectified current flows[36] dependent on the surface charge were predicted with simulations and measured in select cases with SICM controlled nanopipettes (Fig. 3).[19,20]

In all experiments detailed above, the identity of ions involved has not been considered. Selective ion transport, especially for ions already known to be important in physiology (*e.g.,* potassium, calcium, or protons (local pH)), is often important to measure as well. More complex probe fabrication is a possible solution to enable chemically selective SICM responses. Our group has designed and fabricated pipettes suitable for SICM that possess pH-responsive layers.

Microscale pH probes were fabricated by sequential thermal deposition of Cr and Au on one half of the outer surface of a pipette, followed by parylene C insulation and electropolymerization of a responsive polyaniline (PANi) film.[18] The dynamic range for these micro pH probes was found to be 2.5-12.0 in bulk electrolyte solutions and the sensitivity of the probe ranged from 0.02 – 0.2 ΔpH. For ion selective SICM, microscale pH probes and porous membrane samples were configured as described for four-electrode SICM above. Additionally, the Au/PANi probe was connected to a differential amplifier to record the EMF response related to local $H^+$ concentration. Concentration gradients of $H^+$ and transmembrane potential were used to obtain transmembrane pH differences. Local pH gradients were measured with the microscale pH probe and a potential map over a porous membrane (apparent ΔpH map) was generated. These ion-selective SICM studies and probe fabrication techniques provide a general route to study selective ion transport with high spatial resolution, where selectivity in the measurement is conveyed via a chemically selective coating on the pipette exterior.

## Hybrid SECM-SICM

SICM excels at hybrid techniques (such as P-SICM described above), where the SICM function controls position of the probe and a second auxiliary signal is recorded. SICM can be easily coupled to SECM in this manner and can compensate for the lack of chemical specificity of SICM.[17,37,38] In our studies, we have coupled SECM with SICM to investigate the diffusion and migration of redox active anions and cations ions through single pores in a membrane (Fig. 4 a-c).[17]

The nanopipet probe for SECM-SICM was fabricated in a similar manner as the ion-selective probe described above. Thermal deposition of a Cr adhesion layer followed by a Au layer was performed for one half of nanopipette, and an insulation layer of parylene C was coated on the outside of the whole probe, except the tip region, through chemical vapor deposition (Fig. 4d). Again, a four-electrode SICM configuration was used. The fifth electrode, a Au film electrode, was biased with respect to the reference electrode and the faradaic current was recorded. Polyimide membranes with single pores were mounted between two chambers of a perfusion cell, where redox mediators ferricyanide ($Fe(CN)_6^{3-/4-}$) or ruthenium hexamine ($Ru(NH_3)_6^{3+/4+}$) were only present in the lower chamber. Transmembrane potential-driven migration showed selectivity due to the polarity of the working electrode placed in the lower chamber and the charge of the ions. This SECM-SICM hybrid technique allows ion-selective SICM to be performed for redox ions and therefore affords the chance to study more complex ion transport mechanisms. Recently, we have also adopted methods to prepare a variety of carbon electrode geometries through a combination of parylene CVD and electrode shaping with a focused ion beam (Fig. 4e). We hope these electrodes of well-defined geometry will extend the utility of quantification of SECM/SICM experiments.

## Conclusion and Future Direction

SICM is a versatile tool for nanoscale ion-transport studies. Through modification of the instrument and experimental setup, and selective application of concentration gradients or transmembrane potentials, new modes to study ion transport can be realized. Potentiometric measurements have improved the sensitivity of local conductance recordings and operate under biologically relevant conditions, to enable studies of ion transport in living-systems. Further advances based on probe fabrication and hybrid techniques have made SICM more powerful in nanoscale ion transport studies by adding chemical specificity.

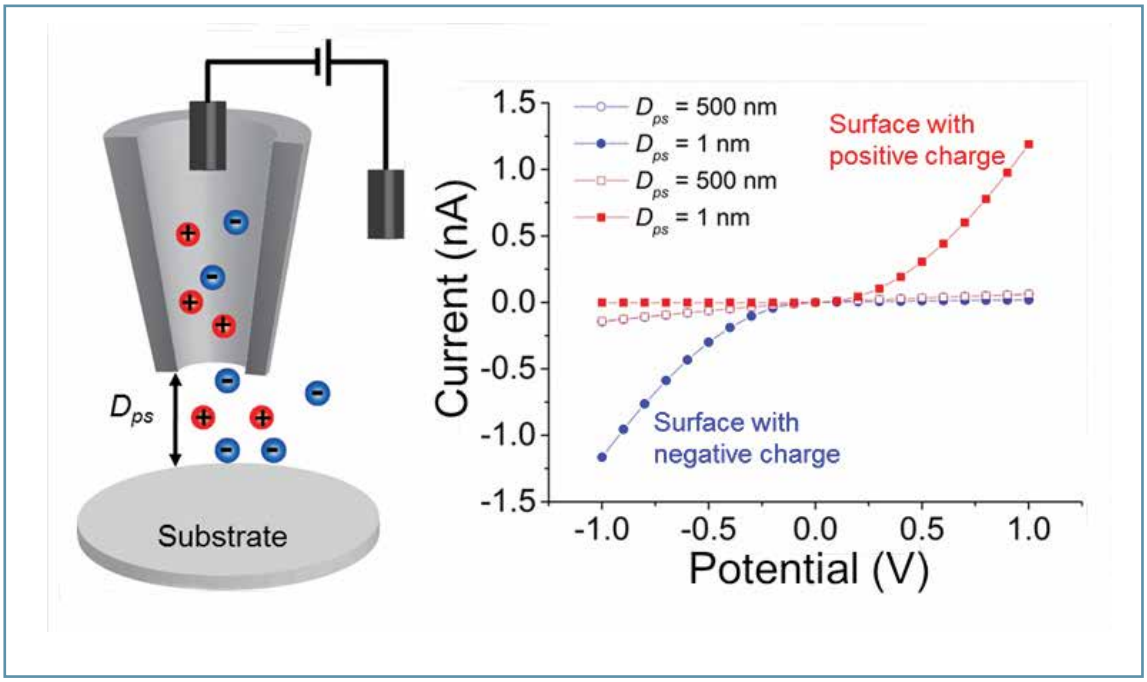


**Fig. 3.** Cartoon representation (left) and simulated data (right) for transduction of surface charge with a nanopipette. (Portions of figure adapted with permission from reference [20].)

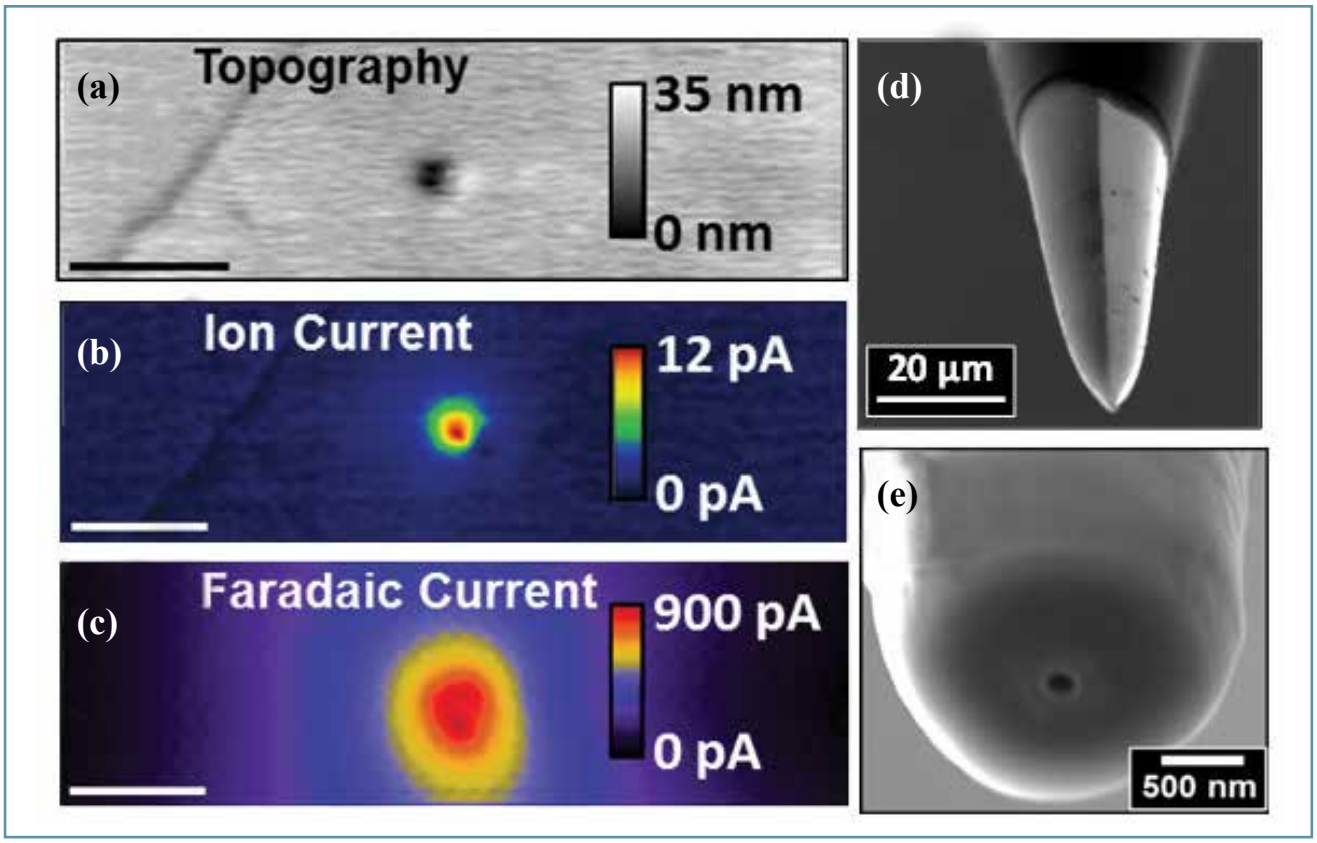


**Fig. 4.** *(a) Topography imaged with the nanopipet-electrode of a 900 nm pore in the polyimide membrane. (b) Ion current and (c) faradaic current of* $Fe(CN)_6^{3-/4-}$ *reduction recorded with the AuE as the pore was imaged. All images were recorded simultaneously with a transmembrane potential of -300 mV vs. Ag/AgCl and a probe-surface distance of 120 nm. Scale bar in all images is 2.0 µm. (d) Scanning electron micrograph of nanopipet-electrode with an exposed electrode area of 3.8 x* $10^3$ $\mu m^2$ *and a clear distinction between the Au electrode (right), quartz (left) and parylene-c insulation (top). (e) SEM micrograph of a carbon ring/nanopore electrode with a 165 nm (diameter) nanopore. Outer and inner radii of the carbon ring electrode are 278 nm and 135 nm, respectively. (Portions of figure and caption adapted with permission from references [17] and [21].)*

Although SICM has proven a good tool for investigation of ion transport at small scales, there are still several limitations. First, efforts to improve spatial and temporal resolution are necessary to extend application of SICM towards more challenging biological samples. Ion transport through transmembrane ion channels (as opposed to cell-cell junctions described here) is a central issue in biology and physiology. Due to the size of ion channels and their dynamic nature, special efforts to measure ion channels in a non-patched SICM configuration will be required. Although the best-recorded lateral resolution of SICM is approximately 3-6 nm,[39] typical lateral resolution of SICM is on the order of tens of nanometers and is highly dependent on probe size and sample. The scanning process of SICM also produces some limits in temporal resolution for image collection, however, additional scanning methods have lessened the time required per image.[40-42] This same issue, the time response of the image and data collection, is encountered in point measurements such as the conductance studies shown above. Future efforts to generate potential maps of samples, to achieve fast data acquisition and minimize instrument drift are under way in our lab. Further, our past efforts have focused primarily on biological samples, but the same tool set we are developing can also be brought to bear on abiotic systems, for instance membranes in fuel cells or in battery materials where ion transport is of interest.

Taken as a whole, SICM provides opportunities to measure electrochemical processes in a complementary and – in some cases – superior fashion to other electrochemical imaging techniques. Further, we can expect that additional functionalities afforded by SICM, which include *in situ* dosing/deposition[43,44] and nanopipette mass spectrometry,[45] will comingle with electrochemical studies. In addition to SICM, recent reports of high resolution SECM studies[43,44] and hybrid or modified SECM/SICM techniques[48-50] point to a resurgence in electrochemical imaging platforms, which open new vistas to studies of electrochemical processes at interfaces.

## About the Authors


**Lushan Zhou** studied chemistry as an undergraduate at Peking University, and joined the Baker Group at Indiana University in the fall of 2012. She is a member of the Indiana Student Chapter of the ECS. Her research interests include new imaging modes of scanning ion conductance microscopy. She may be reached at luszhou@indiana.edu.

**Yi Zhou** received her BS in chemistry from Zhejiang University in 2009 and joined the Baker Group in the fall at Indiana University. She is a member of the Indiana Student Chapter of the ECS. Her research focuses on the study of heterogeneous ion transport in synthetic and biological membranes with scanning ion conductance microscopy. She may be reached at yz26@indiana.edu.


*(continued on next page)*

**Lane A. Baker** is a James F. Jackson Associate Professor at Indiana University, Bloomington, IN, USA. He received his BS in chemistry from Missouri State University, and his PhD Texas A&M University. He is an active member of The Electrochemical Society and is a faculty sponsor for the local Indiana Student Chapter of the ECS. His research interests involve fundamental and applied investigations of electrochemistry, bioanalytical chemistry and nanotechnology. He may be reached at lanbaker@indiana.edu.

## References

1. A. J. Bard, G. Denuault, C. Lee, D. Mandler, and D. O. Wipf, *Acc. Chem. Res.,* **23**, 357 (1990).
2. A. J. Bard, F. R. F. Fan, J. Kwak, and O. Lev, *Anal. Chem.,* **61**, 132 (1989).
3. A. J. Bard, F. R. F. Fan, D. T. Pierce, P. R. Unwin, D. O. Wipf, and F. M. Zhou, *Science*, **254**, 68 (1991).
4. J. Kwak and A. J. Bard, *Anal. Chem.*, **61**, 1221 (1989).
5. C. M. Lee, J. Y. Kwak, and A. J. Bard, *PNAS*, **87**, 1740 (1990).
6. H.-Y. Liu, F. F. Fan, C. W. Lin, and A. J. Bard, *J. Am. Chem. Soc*., **108**, 3838 (1986).
7. R. C. Engstrom and C. M. Phar, *Anal. Chem*., **61**, 1099A (1989).
8. R. C. Engstrom, M. Weber, D. J. Wunder, R. Burgess, and S. Winquist, *Anal. Chem*., **58**, 844 (1986).
9. S. C. S. Lai, J. V. Macpherson, and P. R. Unwin, *Mater. Res. Bull.,* **37**, 668 (2012).
10. D. Koley, M. M. Ramsey, A. J. Bard, and M. Whiteley, *PNAS*, **108**, 19996 (2011).
11. P. K. Hansma, B. Drake, O. Marti, S. A. C. Gould, and C. B. Prater, *Science*, **243**, 641 (1989).
12. A. I. Shevchuk, P. Novak, Y. Takahashi, R. Clarke, M. Miragoli, B. Babakinejad, J. Gorelik, Y. E. Korchev, and D. Klenerman, *Nanomedicine*, **6**, 565 (2011).
13. C.-C. Chen and L. A. Baker, *Analyst*, **136**, 90 (2011).
14. C.-C. Chen, M. A. Derylo, and L. A. Baker, *Anal. Chem.*, **81**, 4742 (2009).
15. C.-C. Chen, Y. Zhou, and L. A. Baker, *ACS Nano*, **5**, 8404 (2011).
16. C.-C. Chen, Y. Zhou, C. A. Morris, J. Hou, and L. A. Baker, *Anal. Chem.*, **85**, 3621 (2013).
17. C. A. Morris, C.-C. Chen, and L. A. Baker, *Analyst*, **137**, 2933 (2012).
18. C. A. Morris, C.-C. Chen, T. Ito, and L. A. Baker, *J. Electrochem. Soc.*, **160**, H430 (2013).
19. N. Sa and L. A. Baker, *J. Am. Chem. Soc.*, **133**, 10398 (2011).
20. N. Sa, W.-J. Lan, W. Shi, and L. A. Baker, *ACS Nano*, **7**, 11272 (2013).
21. R. Thakar, A. E. Weber, C. A. Morris, and L. A. Baker, *Analyst*, **138**, 5973 (2013).
22. Y. Zhou, C.-C. Chen, and L. A. Baker, *Anal. Chem.*, **84**, 3003 (2012).
23. N. Lakshminarayanaiah, *Equations of Membrane Biophysics*; Academic Press, Inc.: Orlando, FL, 1984.
24. Y. E. Korchev, C. L. Bashford, M. Milovanovic, I. Vodyanoy, and M. J. Lab, *Biophys. J.*, **73**, 653 (1997).
25. E. Frömter, *J. Membr. Biol.*, **8**, 259 (1972).
26. M. Cereijido, E. S. Robbins, W. J. Dolan, C. A. Rotunno, and D. D. Sabatini, *J. Cell Biol.*, **77**, 853 (1978).
27. M. Cereijido, E. Stefani, and A. Martinezpalomo, *J. Membr. Biol.*, **53**, 19 (1980).
28. E. Frömter and J. Diamond, *Nature: New biology*, **235**, 9 (1972).
29. M. Cereijido and J. M. Anderson, *Tight Junctions*; 2 ed.; CRC Press: New York, 2001.
30. M. Cereijido, L. Gonzalez-Mariscal, and L. Borboa, *J. Exp. Biol.*, **106**, 205 (1983).
31. A. S. L. Yu, M. H. Cheng, S. Angelow, D. Guenzel, S. A. Kanzawa, E. E. Schneeberger, M. Fromm, and R. D. Coalson, *J. Gen. Physiology*, **133**, 111 (2009).
32. M. Cereijido, E. Stefani, and B. C. Deramirez, *J. Membr. Biol.*, **70**, 15 (1982).
33. P. Florian, T. Schoneberg, J. D. Schulzke, M. Fromm, and A. H. Gitter, *J. Physiol. (London)*, **545**, 485 (2002).
34. A. H. Gitter, K. Bendfeldt, J. D. Schulzke, and M. Fromm, *Pfluegers Archiv - European Journal of Physiology*, **439**, 477 (2000).
35. A. H. Gitter, M. Bertog, J. D. Schulzke, and M. Fromm, *Pfluegers Archiv - European Journal of Physiology*, **434**, 830 (1997).
36. Z. S. Siwy and S. Howorka, *Chem. Soc. Rev.*, **39**, 1115 (2010).
37. D. J. Comstock, J. W. Elam, M. J. Pellin, and M. C. Hersam, *Anal. Chem.*, **82**, 1270 (2010).
38. Y. Takahashi, A. I. Shevchuk, P. Novak, Y. Murakami, H. Shiku, Y. E. Korchev, and T. Matsue, *J. Am. Chem. Soc.*, **132**, 10118 (2010).
39. A. I. Shevchuk, G. I. Frolenkov, D. Sanchez, P. S. James, N. Freedman, M. J. Lab, R. Jones, D. Klenerman, and Y. E. Korchev, *Angew. Chem., Int. Ed. Engl.,* **45**, 2212 (2006).
40. P. Novak, C. Li, A. I. Shevchuk, R, Stepanyan, M. Caldwell, S. Hughes, T. G. Smart, J. Gorelik, V. P. Ostanin, M. J. Lab, G. W. J. Moss, G. I. Frolenkov, D. Klenerman, and Y. E. Korchev, *Nat. Methods*, **6**, 279 (2009).
41. A. Zhukov, O. Richards, V. Ostanin, Y. Korchev, and D. Klenerman, *Ultramicroscopy*, **121**, 1 (2012).
42. Y. Takahashi, Y. Murakami, K. Nagamine, H. Shiku, S. Aoyagi, T. Yasukawa, M. Kanzaki, and T. Matsue, *Phys. Chem. Chem. Phys.*, **12**, 10012 (2010).
43. P. Actis, M. M. Maalouf, H. J. Kim, A. Lohith, B. Vilozny, R. A. Seger, and N. Pourmand, *ACS Nano*, **8**, 546 (2014).
44. P. Actis, S. Tokar, J. Clausmeyer, B. Babakinejad, S. Mikhaleva, R. Cornut, Y. Takahashi, A. L. Cordoba, P. Novak, A. I. Shevchuck, J. A. Dougan, S. G. Kazarian, P. V. Gorelkin, A. S. Erofeev, I. V. Yaminsky, P. R. Unwin, W. Schuhmann, D. Klenerman, D. A. Rusakov, E. V. Sviderskaya, and Y. E. Korchev, *ACS Nano*, **8**, 875 (2014).
45. E. M. Yuill, N. Sa, S. J. Ray, G. M. Hieftje, and L. A. Baker, *Anal. Chem.*, **85**, 8498 (2013).
46. F. O. Laforge, J. Velmurugan, Y. Wang, and M. V. Mirkin, *Anal. Chem.*, **81**, 3143 (2009).
47. M. Shen, R. Ishimatsu, J. Kim, and S. Amemiya, *J. Am. Chem. Soc.*, **134**, 9856 (2012).
48. Y. Takahashi, A. I. Shevchuk, P. Novak, B. Babakinejad, J. Macpherson, P. R. Unwin, H. Shiku, J. Gorelik, D. Klenerman, Y. E. Korchev, and T. Matsue, *PNAS*, **109**, 11540 (2012).
49. N. Ebejer, A. G. Gueell, S. C. S. Lai, K. McKelvey, M. E. Snowden, and P. R. Unwin, *Annu. Rev. Anal. Chem.*, **6**, 329 (2013).
50. K. McKelvey, D. Perry, J. C. Byers, A. W. Colburn, and P. R. Unwin, *Anal. Chem.*, **86**, 3639 (2014).